Surface Charge Effects on Voltammetry in Carbon Nanocavities

Je Hyun Bae,[†], Dengchao Wang,[†] Keke Hu,[†,‡] and Michael V. Mirkin [†,‡,]*

†Department of Chemistry and Biochemistry, Queens College, Flushing, NY 11367

‡The Graduate Center of CUNY, New York, NY 10016

Corresponding Author

E-mail: mmirkin@qc.cuny.edu

FAX: 718-997-5531

ABSTRACT

Ion transport controlled by electrostatic interactions is an important phenomenon in biological and artificial membranes, channels, and nanopores. Here, we employ carbon-coated nanopipettes (CNPs) for studying permselective electrochemistry in a conductive nanopore. A significant accumulation (up to 2000-fold) of cationic redox species and anion depletion inside a CNP by diffuse layer and surface charge effects in solution of low ionic strength were observed as well as the shift of the voltammetric mid-peak potential. Finite-element simulations of electrostatic effects on CNP voltammograms show permselective ion transport in a single conducting nanopore and semi-quantitatively explain our experimental data. The reported results are potentially useful for improving sensitivity and selectivity of CNP sensors for ionic analytes.

Electrochemical processes inside conductive nanopores, nanogaps, and cavities have attracted significant interest because of their relevance to sensors,[1-5] energy conversion/storage,[6,7] DNA sequencing[8] and protein detection,[9] and physicochemical experiments at the level of single molecules.[10-12] Due to the nanometer-scale dimensions and large conductive surface-to-volume ratio, the electrical double layer (EDL) and surface charge effects are more significant in nanopores and nanogaps than in macroscopic electrochemical systems.[3,13-16] The presence of surface-bound excess charge within a nanocavity can result in significant ion accumulation/depletion in solution, ionic adsorption, and permselective behavior. For instance, significant accumulation (and depletion) of ions and ionic adsorption were recently observed in glass and quartz nanopores,[17,18] nanometer-sized thin layer cells (TLC),[19] and microfluidic channels.[20] These processes can be controlled by chemical functionalization that changes the surface charge.[21,22]

The surface charge of nanopores and nano-TLCs influences the distribution and transport of charged redox species.[19,23] The surface charge repels co-ions while counter-ions became the predominant ionic species and accumulate, which affects the charge-permselectivity of such nanostructures. To prepare a single conductive nanopore, the interior wall of the nanocapillary can be coated with conductive materials such as gold,[2,3,5,24] Pt,[25] carbon,[26] or conductive polymers.[27] The applications of conductive nanopipettes in sensing typically involve either recording ion current flowing through the orifice (resistive-pulse and rectification sensing) or amperometric measurements inside the conductive shaft.

Carbon nanopipettes (CNP) were prepared by the Bau and Gogotsi groups using chemical vapor deposition (CVD) of carbon into quartz capillaries.[28,29] By modifying these procedures, we previously produced open CNPs[30] and carbon nanocavity electrodes ("nanosampler"[31]) and

demonstrated their usefulness for resistive-pulse and rectification sensing[30,32] and electroanalysis.[31] When a CNP is immersed in aqueous solution, water gets driven into the pipette by capillary forces. If the solution contains some electroactive species, it can be oxidized at the carbon surface inside the pipette when the CNP potential is scanned in the anodic direction and re-reduced during the cathodic scan. A typical CNP voltammogram consists of a pair of essentially symmetrical peaks indicative of the TLC behavior.[30,31]

CNPs offer a unique environment for studying the effects of nanoconfinement, surface charge, and adsorption on electrochemical processes. Our recent study of ion current rectification in open CNPs[16] revealed high negative charge density (*ca.* -1 to -5 μC/cm^2) on the carbon surface due to deprotonated surface carboxylic groups in neutral aqueous solution. Unlike many reported devices that require sophisticated fabrication and/or chemical surface modification, the fabrication of CNPs is relatively simple, and the charge density can be controlled by varying the applied potential without surface modification. In our previous experiments,[30,31] the supporting electrolyte concentration was high (0.1-1 M), and no possibility of EDL/surface charge effects on CNP voltammograms was considered. However, there are two reasons for electrostatic effects to become significant at low electrolyte concentrations employed in the present study (e.g., 0.1 – 1 mM). First, the carbon surface is known to be negatively charged, and the surface charge has to be compensated by dissolved cations to maintain electroneutrality inside the CNP. For a cylindrical segment of the CNP shaft (cylindrical geometry is assumed here for the sake of simplicity; the actual CNP shaft is conical), the ratio of the total cationic charge in solution to the carbon surface charge is $cFr/2\sigma$, where c is the concentration of the 1:1 electrolyte, F is the Faraday constant, r is the inner CNP radius, and σ is the surface charge density. For a not very narrow section of the CNP with r = 100 nm, c = 1 mM

and relatively small σ = 1 μC/cm^2,[16] this ratio equals 0.5, indicating that significant accumulation of cations and depletion of anions inside the CNP is required for electroneutrality. This simple estimate suggests that a CNP may exhibit permselective responses to charged redox analytes at low electrolyte concentrations. (By contrast, for c = 0.1 M, the volume-to-surface charge ratio is 50, and no significant permselectivity can be expected). The second reason for permselective behavior at low electrolyte concentrations is that the effective EDL thickness at c = 0.1 mM is ~30 nm,[33] i.e. comparable to a typical CNP orifice radius value; and, therefore, the anion permeation can be hindered.[34] Herein we obtain the voltammograms of cationic, neutral and anionic redox species to explore the permselective behavior of CNPs and perform finite-element simulations of these phenomena.

EXPERIMENTAL SECTION

Fabrication of carbon Nanopipettes. Quartz capillaries (1.0 mm o.d., 0.5 mm i.d.) were purchased from Sutter Instrument Co and used to pull nanopipettes with the tip orifice radius from ~20 to ~200 nm by a laser pipette puller (P-2000; Sutter Instruments). A layer of carbon was formed inside of a pre-pulled pipette by CVD at 945-950 °C, using methane as the carbon source and argon as the protector (methane/argon: 1/1), as described previously.[29-31] The CVD time depends on the nanopipette radius, and a longer CVD time is needed for a larger tip radius. TEM images of CNPs were acquired using field emission transmission electron microscope (JEOL 2100F) operated at 200 keV.

Electrochemical experiments. Voltammetric experiments were performed using a CHI model 760E bipotentiostat (CH Instruments, Austin, TX) in the two-electrode setup with a commercial Ag/AgCl (1 M KCl, CHI 111) reference electrode with a porous Teflon tip to minimize the solution leakage or a Ag/AgCl wire reference. All experiments

were carried out at room temperature (22−25 °C) inside a Faraday cage. The appropriate protection was used to avoid electrostatic damage to carbon nanotips.[35] In some experiments, the volume of solution inside CNPs was controlled by a syringe pump (NE-1002X microfluidic syringe pump, New Era Pump Systems Inc.).

RESULTS AND DISCUSSION

CNP voltammograms with excess electrolyte. When the CNP is immersed in solution containing a redox species that can react at its surface, the recorded current initially varies with time, but eventually stabilizes to yield superimposable consecutive voltammetric cycles.[31] The stabilized charging and faradaic currents indicate that the solution volume inside the pipette has attained a stationary value. CNPs were characterized by cyclic voltammetry and TEM. A typical CNP cyclic voltammogram (CV) of FcMeOH (Figure 1A) exhibits a combination of the steady-state voltammetric current at the carbon nanoring exposed to the external solution with a pair of prominent slightly asymmetrical peaks due to the electrochemical reaction of inside the conductive pipette.[31] The former component is represented by a sigmoidal steady-state voltammogram obtained at relatively low sweep rate (e.g., v = 0.1 V/s; curve 1 in Figure 1A). From the diffusion limited steady-state current (~23 pA), the effective radius $a \approx 65$ nm can be evaluated using eq 1 for an inlaid disk

$$i_d = 4xnFDc^*a \quad (1)$$

where n = 1 is the number of transferred electrons, F is the Faraday constant, c^* = 1 mM and D = 7.8×10^{-6} cm^2/s [36] are the bulk concentration and the diffusion coefficient of FcMeOH, respectively. The factor x is a function of RG;[37] x = 1.16 corresponds to RG = 1.5 (i.e. the ratio of glass radius to that of the conductive tip) typical of thick-wall quartz pipettes used in this study (An ~10% difference between the diffusion currents to the open CNP and the disk

electrode of the same radius[31] is within the uncertainty margin due to the imperfect tip geometry and variations in RG value). A similar *a* value (~70 nm) was obtained from the TEM image (Figure 1B) of the same CNP.

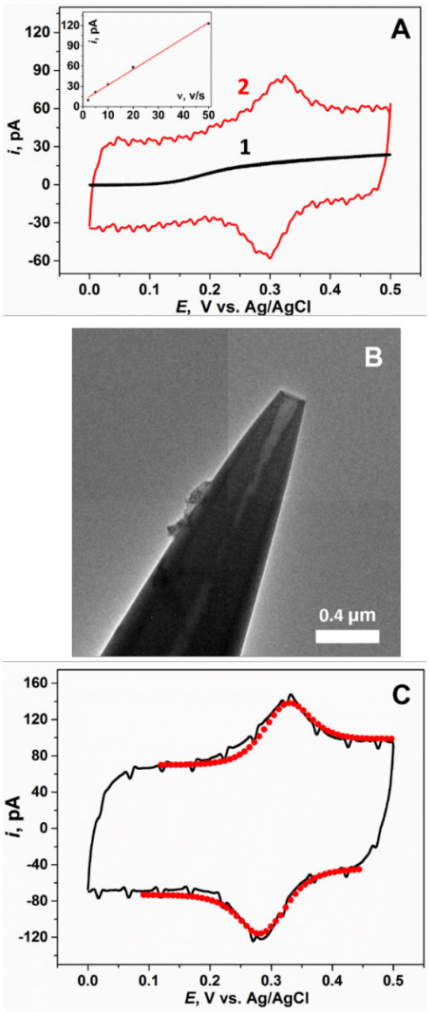

Figure 1. (A) CVs of 1 mM FcMeOH in 1 M KCl solution obtained using a 65 nm radius open CNP at different potential scan rates. *v*, V/s = 0.1 (1) and 10 (2). The inset shows the scan rate dependence of the anodic peak current. (B) TEM image of the same CNP after electrochemical experiments. (C) Simulated (symbols) and experimental (solid line) CVs at *v* = 20 V/s.

The two peaks obtained at a faster potential sweep rate (e.g., *v* = 10 V/s; curve 2 in Figure 1A) are due to the complete oxidation/reduction of FcMeOH molecules inside the carbon-coated pipette shaft. As discussed earlier,[31] the peak current is directly proportional to *v* (the inset in

Figure 1A). The effective CNP volume (V_p = 2.5 fL) was estimated from the integrated charge (Q) under the oxidation or reduction peak after background subtraction using Eq. (2)

$$V_p = Q/(F^*c^\circ) \quad (2)$$

where c° is the FcMeOH concentration inside the CNP. With a = 65 nm and the 5° pipette angle, the corresponding effective depth of the cavity is *ca*. 6 μm, i.e. ~90a. The CV simulated for these geometric parameters and v = 20 V/s (red curve in Figure 1C) fits very well the experimental voltammogram (black curve in Figure 1C) after the charging current subtraction. The electrical noise in Figs. 1A and C is due to the high filter frequency (15 kHz) used to avoid distortions in fast scan CVs.

The V_p value is reasonably reproducible in repeated experiments, as demonstrated by the data shown in Figure S1. After each experiment, the pipette was washed and dried and re-immersed in the same solution for the next measurement. The average effective volume from five consecutive measurements is V_p = 0.58 pL ± 0.07 pL. With a = 50 nm and the 5° pipette angle, the corresponding effective depth of the cavity is *ca*. 41 μm, i.e. ~820a.

Effects of low electrolyte concentration. Because of the negatively charged carbon surface and the resulting EDL structure, the cations are expected to be enriched while the anions should be depleted inside the CNP. The ion distribution near the charged carbon surface (σ = -0.7 μC/cm^2) simulated for the 1 mM bulk concentration of the 1:1 electrolyte (Figure 2A) shows the increased cation concentration, [c^+] ≈ 12 mM near the carbon surface, while the anions are almost totally depleted ([c^-] ≈ 0 mM). Such ion enrichment and depletion could be used for selective and sensitive determination of ionic redox species.

The effect of the electrolyte concentration is seen from CVs simulated for high (1 M) and low (1 mM) electrolyte concentrations, σ = -0.7 μC/cm^2 on the carbon surface, and four redox

species with different charges and standard potentials (FcMeOH, $FcTMA^+$, $Ru(NH_3)_6^{3+}$ and $Fe(CN)_6^{4-}$ in Figures 2B-2E, respectively). In 1 M KCl solution, there is enough cations to compensate the excess negative surface charge on the carbon surface, so that the concentration of ionic redox species inside the CNP is close to its bulk value; whereas in 1 mM KCl the local concentrations of both the electrolyte and charged redox species are strongly affected by the surface charge, i.e. cationic redox species should be accumulated and the anions – depleted within the CNP. One should notice that the simulated charge density is potential dependent. The applied potential is supposed to change the effective surface charge, depending on the specific capacitance of the carbon/solution interface (see Supporting Information for simulation details).

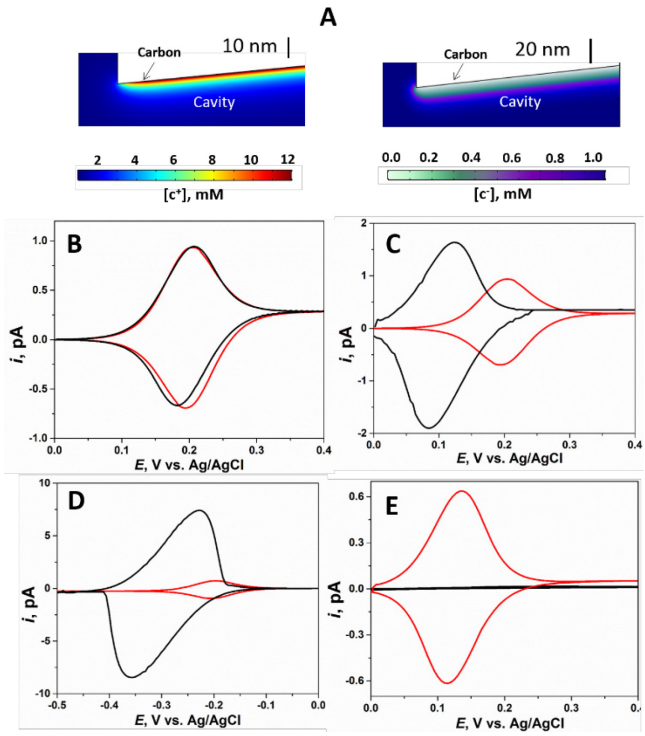

Figure 2. (A) Simulated concentration distribution of the cations (left panel) and anions (right panel) inside a 65-nm-radius CNP. The bulk value for the c^+ and c^- in the outer solution is 1 mM. (B) – (E) CNP CVs of different redox species simulated for 10 μM of (B) FcMeOH, (C) $FcTMA^+$, (D) $Ru(NH_3)_6^{3+}$, and (E) $Fe(CN)_6^{4-}$ in either 1 M (red curves) or 1 mM (black curves) KCl solution. a = 65 nm; the pipette angle is 5°; the effective depth of the cavity is 300a; v = 1 V/s; σ = -0.7 μC/cm^2.

In Figure 2B, the anodic and cathodic peak currents for neutral FcMeOH redox species are similar in 1 M and 1 mM KCl (red and black curves), and a slight negative potential shift (~-20 mV) can be seen in the reduction peak of $FcMeOH^+$. The double layer effects are much stronger for the cationic $FcTMA^{+/2+}$ couple (Figure 2C). A significant increase in concentration of $FcTMA^+$ inside the negatively charged CNP cavity filled with 1 mM KCl leads to the higher anodic and cathodic peak currents, and the mid-peak potential shifts towards more negative values. Simulated dependences of the accumulation of ionic redox species on pipette size and surface charge are shown in Figs. S2 and S3, respectively. The higher the surface charge density and the smaller the pipette radius the stronger the cation accumulation in CNPs.

The surface effect on the voltammograms becomes stronger for the multivalent redox species, as shown in the panels D and E. A large increase in the peak currents of $Ru(NH_3)_6^{3/2+}$ in 1 mM KCl resulted in a significant resistive potential drop inside the CNP and the increased peak potential splitting (black curve in Figure 2D). In contrast, the $Fe(CN)_6^{4-}$ current in 1 mM KCl is negligibly low (black curve in Figure 2E) due to the anion depletion. The mid-peak potential shift in the negative direction at a low electrolyte concentration is most prominent for $Fe(CN)_6^{4/3-}$ (this effect cannot be seen in Figure 2E because of the greatly suppressed signal).

Cation accumulation in CNPs. The experimental CVs in Figure 3 exhibit essential features predicted by simulations. In 1 M KCl solution containing equal concentrations (1 μM) of FcMeOH and $Ru(NH_3)_6^{3+}$, the two pairs of anodic and cathodic peaks show comparable magnitudes of peak currents and mid-point potentials corresponding to the formal potentials of both redox couples (red curve in Figure 3A). In the CV obtained with the same CNP under the same conditions except a much lower ionic strength (1 mM KCl; black curve in Figure 3A), the changes in FcMeOH response are minor, but the oxidation/reduction charge calculated from the

second pair of peaks suggests *ca.* 40-fold accumulation of $Ru(NH_3)_6^{3+}$ inside the CNP. A similar trend is observed for $FcTMA^{+}/FcTMA^{2+}$ whose concentration increased by the factor of two when 1 M KCl electrolyte was replaced with 1 mM KCl (Figure S4). The accumulation of the $FcTMA^{2+/+}$ was smaller than that of $Ru(NH_3)_6^{3+/2+}$ because of the lower positive ionic charges of the former redox couple and the larger CNP orifice.

Ion accumulation in CNPs enables trace-level analysis. Figure 3B shows a CV obtained

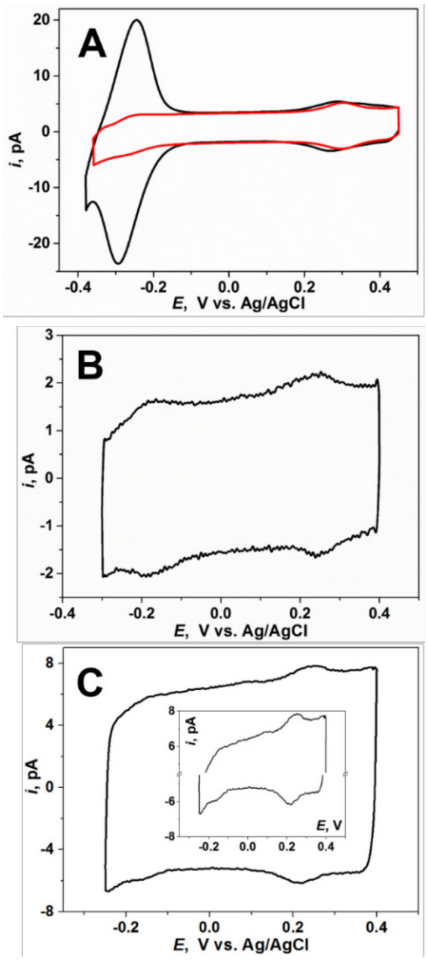

Figure 3. CNP voltammograms of FcMeOH and $Ru(NH_3)_6^{3+}$ obtained in 1 mM KCl (black curves) and 1 M KCl (red curve in A) solutions. The bulk concentrations of FcMeOH and $Ru(NH_3)_6^{3+}$ are: 1 μM and 1 μM (A), 1 μM and 10 nM (B), 100 nM and 10 pM (C), respectively. v = 200 mV/s. a, nm = 33 (A), 68 (B), and 82 (C). The inset in (C): anodic and cathodic peaks magnified for better clarity.

in a 1 mM KCl solution containing 1 μM FcMeOH and the 10 nM $Ru(NH_3)_6^{3+}$. With the bulk concentration ratio of 100 times, the amount of $Ru(NH_3)_6^{3+}$ in the CNP is about 1.5 that of FcMeOH, corresponding to ~150-fold cation accumulation. A pair of small peaks in Figure 3C was obtained with the bulk concentration of $Ru(NH_3)_6^{3+}$as low as 10 pM. From comparison to the peaks in the same CV produced by 100 nM FcMeOH, the accumulation of $Ru(NH_3)_6^{3+}$ is ~2000-fold. An even greater accumulation and lower detection limit can be expected for polycations with a charge higher than that of $Ru(NH_3)_6^{3+}$ and smaller CNPs. Based on our simulations, such enormous ion accumulation cannot be attributed to the surface charge effect in a relatively large (a = 82 nm) CNP. An additional source of signal amplification must be the microporous structure of the partially amorphous carbon layer. Since the dimensions of micropores are much smaller those of the CHP inside, the ion accumulation effect in them should be much stronger. The lack of information about average porosity of the carbon film, pore size distribution and permeability to various ions and water precludes quantitative modeling of the effect of micropores on ion accumulation.

Anion depletion in CNPs. The negative surface charge is expected to lower the concentrations of anions near the carbon surface in the CNP cavity (Figure 2A, right panel) and suppress the voltammetric response of anionic redox species, such as $Fe(CN)_6^{4-}$ (Figure 2E). As discussed above, this effect becomes much stronger at lower electrolyte concentration and smaller CNP radius (Figure 4). Using a 51-nm-radius CNP, the 35-fold $Fe(CN)_6^{4-}$ depletion was obtained in 0.1 mM KCl (black curve in Figure 4A) as compared to the CV in 1 M KCl (red curve). With a smaller CNP (a = 14 nm; Figure 4B), both anodic and cathodic peaks of $Fe(CN)_6^{4/3-}$ in 0.1 mM KCl are completely suppressed, i.e. the anion depletion in this case is much larger than 35-fold (*cf.* Figure 4A). The ~30 nm diffuse layer thickness in 0.1 mM KCl[33]

is significantly larger than the 14 nm radius of the CNP orifice, greatly impeding the flux of multicharged anions. In combination with the anion exclusion from the negatively charged nanocavity, this strong electrostatic barrier results in the negligibly low voltammetric current of $Fe(CN)_6^{4-}$. The ferrocyanide signal is recovered at 1 M KCl, where the diffuse layer thickness is much smaller than *a* (red curve in Figure 4B).

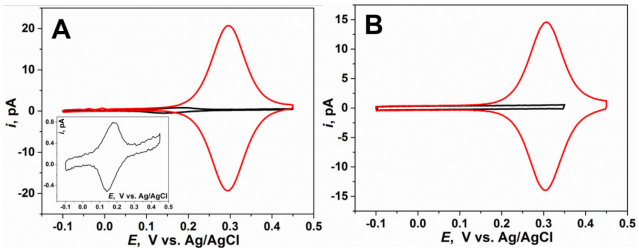

Figure 4. Cyclic voltammograms of 10 μM $Fe(CN)_6^{4-}$ in different KCl solutions obtained using a 51 nm (A) and 14 nm (B) radius CNP. The inset in A shows a zoom-in of the black curve. *v*, mV/s = 5 (A) and 50 (B). KCl, mM = 0.1 (black curves) and 1000 (red curves)

Another salient feature in CNP voltammograms of $Fe(CN)_6^{4-}$ at a low electrolyte concentration is a significant (~150 mV in Figure 4A) shift of the mid-peak potential in the negative direction. This shift (also predicted by simulations) cannot be explained by liquid junction potential whose value is only 8.4 mV (for the 0.1 mM KCl / 1 M KCl junction). This phenomenon along with the permselective behavior can be used to fine tune the CNP response to selectively detect analytes and suppress interferences.

A CNP CV shown in Figure 5A was obtained in 0.1 mM KCl containing 1 μM $Fe(CN)_6^{4-}$ and 1 μM $FcTMA^+$. The only pair of peaks in this voltammogram corresponds to oxidation/reduction of $FcTMA^{+/2+}$ occurring at ~0.4 V vs Ag/AgCl, i.e. close to the half-wave potential of the $FcTMA^+$ oxidation at the carbon microdisk electrode (Figure 5B). In contrast to the steady-state voltammogram (Figure 5B) in which the heights of $FcTMA^+$ and $Fe(CN)_6^{4-}$ waves are similar, the $Fe(CN)_6^{4/3-}$ signal in the CNP voltammogram is completely suppressed.

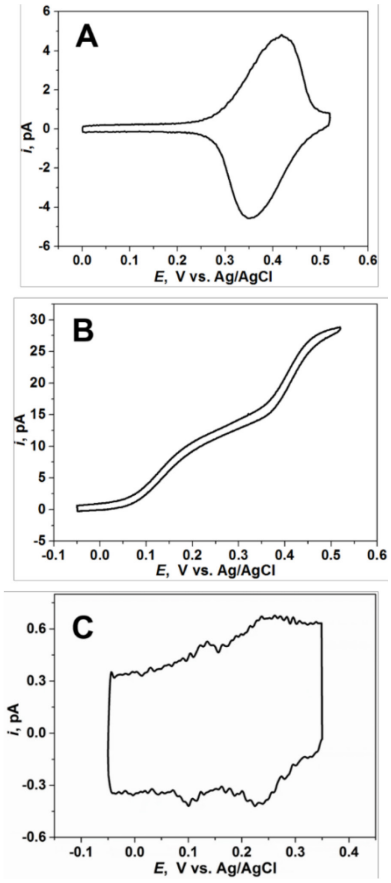

Figure 5. Voltammograms of mixtures of redox species at carbon electrodes. (A) CNP CV of 1 μM $Fe(CN)_6^{4-}$ and 1 μM $FcTMA^+$ in 0.1 mM KCl. a = 130 nm. (B) Steady-state voltammogram of 10 μM $Fe(CN)_6^{4-}$ and 10 μM $FcTMA^+$ at a 5 μM radius carbon disk electrode in 1 mM KCl. (C) CNP CV of 50 μM $Fe(CN)_6^{4-}$ and 5 μM FcMeOH in 0.1 mM KCl. a = 23 nm. v, mV/s = 10 (A and B) and 50 (C).

In Figure 5C, the solution contained a mixture of 50 μM $Fe(CN)_6^{4-}$ and 5 μM FcMeOH in 0.1 mM KCl. With only 80 mV difference between their formal potentials, the 10 times higher concentration of $Fe(CN)_6^{4-}$ would have completely obscured the wave of FcMeOH oxidation in a conventional voltammetric experiment. By contrast, the $Fe(CN)_6^{4/3-}$ response in a CNP CV (Figure 5C) is diminished and the mid-peak potential is shifted towards more negative values, so that FcMeOH can readily be measured.

CONCLUSIONS

Because of the negatively charged carbon surface, CNPs exhibit strong permselectivity at low electrolyte concentrations. The significant accumulation of cations and depletion of anions within the carbon nanocavity are predicted by simulations and observed experimentally. As expected,[38] the magnitude of these effects increases with the ionic charge. The electrostatic effects can be used for trace analysis of ionic redox species and elimination of charged interferences. Thus, the 2000 fold accumulation of $Ru(NH_3)_6^{3+}$ inside the CNP enabled the detection of this species at the level of 10 pM, while the current produced by 10^6 times higher concentration of $Fe(CN)_6^{4-}$ was completely suppressed. The advantages of CNP-based electrochemical nanosensors, such as a recently reported sensor for dopamine,[39] include the small physical size, improved sensitivity and selectivity along with a relatively simple fabrication protocol not requiring expensive lithography or labor intense synthesis. It should be possible to reverse the permselectivity of a CNP by changing the polarity of the surface charge by using a different composition of the gas mixture in CVD fabrication or via chemical modification of the carbon wall.[22]

At high electrolyte concentrations, when the double layer effects are relatively weak, a quantitative fit can be achieved between the simulated and experimental CNP CVs (see, e.g., Figure 1C). In contrast, the simulations for a low electrolyte concentrations provide only semi-quantitative description of the CNP response because several parameters required for exact modeling (e.g., carbon surface change density and porosity) are not currently available. The experimentally observed cation accumulation is typically stronger than that predicted by simulations (especially at very low concentrations, e.g., in Figure 3C), while the mid-peak potential shift in experimental CVs is often less prominent.

ASSOCIATED CONTENT

Supporting Information. Supplemental materials and methods, reproducibility test of solution volume in the CNP, surface charge and size effects on CNP voltammograms, ion accumulation of $FcTMA^+$, time-dependent diffusion problem, and COMSOL simulation report. This material is available free of charge via the Internet at http://pubs.acs.org.

AUTHOR INFORMATION

Corresponding Author

*E-mail: mmirkin@qc.cuny.edu

Author Contributions

All authors have given approval to the final version of the manuscript.

Notes

The authors declare no competing financial interest.

ACKNOWLEDGMENTS

The support of this work by the National Science Foundation (CHE-1763337) is gratefully acknowledged. We thank Dr. Huolin Xin (Center for Functional Nanomaterials at Brookhaven National Laboratory) for assistance with TEM imaging.

REFERENCES

(1) Fan, Y.; Anderson, T. J.; Zhang, B. Single-molecule electrochemistry: From redox cycling to single redox events. *Curr. Opin. Electrochem.* **2018,** *7*, 81-86.

(2) Freedman, K. J.; Otto, L. M.; Ivanov, A. P.; Barik, A.; Oh, S. H.; Edel, J. B. Nanopore sensing at ultra-low concentrations using single-molecule dielectrophoretic trapping. *Nat. Commun.* **2016,** *7*. 10217.

(3) Yang, C.; Hinkle, P.; Menestrina, J.; Vlassiouk, I. V.; Siwy, Z. S. Polarization of Gold in Nanopores Leads to Ion Current Rectification. *J. Phys. Chem. Lett.* **2016,** *7*, 4152-4158.

(4) Yu, R.-J.; Ying, Y.-L.; Gao, R.; Long, Y.-T. Confined Nanopipette Sensing: From Single Molecules, Single Nanoparticles, to Single Cells. *Angew. Chem.-Int. Edit.* **2018,** doi: 10.1002/anie.201803229.

(5) Xu, X. L.; He, H. L.; Jin, Y. D. Facile One-Step Photochemical Fabrication and Characterization of an Ultrathin Gold-Decorated Single Glass Nanopipette. *Anal. Chem.* **2015,** *87*, 3216-3221.

(6) Gogotsi, Y. What Nano Can Do for Energy Storage. *ACS Nano* **2014**, *8*, 5369–5371.

(7) Li, W.; Liu, J.; Zhao, D. Mesoporous materials for energy conversion and storage devices. *Nat. Rev. Mater.* **2016,** *1*, 16023-16040.

(8) Farimani, A. B.; Min, K.; Aluru, N. R. DNA Base Detection Using a Single-Layer MoS_2. *ACS Nano* **2014,** *8*, 7914–7922.

(9) Rutkowska, A.; Freedman, K.; Skalkowska, J.; Kim, M. J.; Edel, J. B.; Albrecht, T. Electrodeposition and bipolar effects in metallized nanopores and their use in the detection of insulin. *Anal. Chem.* **2015,** *87*, 2337-2344.

(10) Fan, F.-R. F.; Bard, A. J. Electrochemical detection of single molecules. *Science* **1995**, 267, 871-874.

(11) Sun, P.; Mirkin, M. V. Electrochemistry of Individual Molecules in Zeptoliter Volumes. *J. Am. Chem. Soc.* **2008**, *130*, 8241-8250.

(12) Lemay, S. G.; Kang, S.; Mathwig, K.; Singh, P. S. Single-Molecule Electrochemistry: Present Status and Outlook. *Acc. Chem. Res.* **2013,** *46*, 369-377.

(13) L. Fan, Y. Liu, J. Xiong, H. S. White, S. Chen, Electron-transfer kinetics and electric double layer effects in nanometer-wide thin-layer cells. *ACS Nano* **2014**, *8*, 10426–10436.

(14) Q. Chen, K. McKelvey, M. A. Edwards, H. S. White, Redox Cycling in Nanogap Electrochemical Cells. The Role of Electrostatics in Determining the Cell Response. *J. Phys. Chem. C* **2016**, *120*, 17251–17260.

(15) Bae, J. H.; Yu, Y.; Mirkin, M. V. Recessed Nanoelectrodes for Nanogap Voltammetry. *ChemElectroChem* **2016**, *3*, 2043–2047.

(16) Wang, D.; Mirkin, M. V. Electron-Transfer Gated Ion Transport in Carbon Nanopipettes. *J. Am. Chem. Soc.* **2017,** *139*, 11654-11657.

(17) He, Y.; Gillespie, D.; Boda, D.; Vlassiouk, I.; Eisenberg, R. S.; Siwy, Z. S. Tuning transport properties of nanofluidic devices with local charge inversion. *J. Am. Chem. Soc.* **2009,** *131*, 5194-5202.

(18) Ali, M.; Nasir, S.; Ramirez, P.; Cervera, J.; Mafe, S.; Ensinger, W. Calcium Binding and Ionic Conduction in Single Conical Nanopores with Polyacid Chains: Model and Experiments. *ACS Nano* **2012,** *6*, 9247-9257.

(19) Lu, J.; Zhang, B. Electrostatic Ion Enrichment in an Ultrathin-Layer Cell with a Critical Dimension between 5 and 20 nm. *Anal. Chem.* **2017,** *89*, 2739-2746.

(20) Pu, Q. S.; Yun, J. S.; Temkin, H.; Liu, S. R. Ion-enrichment and ion-depletion effect of nanochannel structures. *Nano Lett.* **2004,** *4*, 1099-1103.

(21) Daiguji, H. Ion transport in nanofluidic channels. *Chem. Soc. Rev.* **2010,** *39*, 901-911.

(22) Wang, G. L.; Zhang, B.; Wayment, J. R.; Harris, J. M.; White, H. S. Electrostatic-gated transport in chemically modified glass nanopore electrodes. *J. Am. Chem. Soc.* **2006,** *128*, 7679–7686.

(23) Seo, M.; Chung, T. D. Nanoconfinement effects in electrochemical reactions. *Curr. Opinion Electrochem.* **2019**, *13*, 47–54.

(24) Ying, Y. L.; Hu, Y. X.; Gao R.; Yu, R. J.; Gu, Z.; Lee, L. P.; Long, Y. T. Asymmetric Nanopore Electrode-Based Amplification for Electron Transfer Imaging in Live Cells. *J. Am. Chem. Soc.* **2018***, 140*, 5385−5392.

(25) Pan, R.; Xu, M.; Burgess, J. D.; Jiang, D.; Chen, H.-Y. Direct electrochemical observation of glucosidase activity in isolated single lysosomes from a living cell. *Proc. Natl. Acad. Sci. USA* **2018**, *115*, 4087-4092.

(26) Wilde, P.; Quast, T.; Aiyappa, H. B.; Chen, Y. T.; Botz, A.; Tarnev, T.; Marquitan, M.; Feldhege, S.; Lindner, A.; Andronescu, C.; Schuhmann, W. Towards Reproducible Fabrication of Nanometre-Sized Carbon Electrodes: Optimisation of Automated Nanoelectrode Fabrication by Means of Transmission Electron Microscopy. *ChemElectroChem,* **2018***, 5,* 3083-3088.

(27) Perez-Mitta, G.; Marmisolle, W. A.; Trautmann, C.; Toimil-Molares, M. E.; Azzaroni, O. Nanofluidic Diodes with Dynamic Rectification Properties Stemming from Reversible Electrochemical Conversions in Conducting Polymers. *J. Am. Chem. Soc.* **2015,** *137*, 15382-15385.

(28) Kim, B. M.; Murray, T.; Bau, H. H. The fabrication of integrated carbon pipes with sub-micron diameters. *Nanotechnology* **2005**, *16*, 1317–1320.

(29) Singhal, R.; Bhattacharyya, S.; Orynbayeva, Z.; Vitol, E.; Friedman, G.; Gogotsi, Y. Small diameter carbon nanopipettes. *Nanotechnology* **2010**, *21*, 15304.

(30) Hu, K. K.; Wang, Y. X.; Cai, H. J.; Mirkin, M. V.; Gao, Y.; Friedman, G.; Gogotsi, Y. Open Carbon Nanopipettes as Resistive-Pulse Sensors, Rectification Sensors and Electrochemical Nanoprobes. *Anal. Chem.* **2014,** *86*, 8897-8901.

(31) Yu, Y.; Noel, J. M.; Mirkin, M. V.; Gao, Y.; Mashtalir, O.; Friedman, G.; Gogotsi, Y. Carbon Pipette-Based Electrochemical Nanosampler. *Anal. Chem.* **2014,** *86*, 3365-3372.

(32) Wang, Y.; Wang, D.; Mirkin, M. V. Resistive-Pulse and Rectification Sensing with Glass and Carbon Nanopipette. *Proc. R. Soc. A* **2017***, A473,* 20160931.

(33) Bard, A. J.; Faulkner, L. R., *Electrochemical Methods Fundamentals and Applications*. 2nd Ed; John Wiley & Sons, Inc.: 2001, p. 549.

(34) Daiguji, H.; Yang, P. D.; Majumdar, A. Ion Transport in Nanofluidic Channels. *Nano Lett.* **2004,** *4*, 137-142.

(35) Nioradze, N.; Chen, R.; Kim, J.; Shen, M.; Santhosh, P.; Amemiya, S. Origins of Nanoscale Damage to Glass-Sealed Platinum Electrodes with Submicrometer and Nanometer Size. *Anal. Chem.* **2013,** *85*, 6198-6202.

(36) Sun, P.; Mirkin, M. V. Kinetics of Electron Transfer Reactions at Nanoelectrodes. *Anal. Chem.* **2006,** *78*, 6526-6534.

(37) Shoup, D.; Szabo, A. Influence of insulation geometry on the current at microdisk electrodes. *J. Electroanal. Chem.* **1984**, *160*, 27-31.

(38) Hou, C. H.; Taboada-Serrano, P.; Yiacoumi, S.; Tsouris, C. Monte Carlo simulation of electrical double-layer formation from mixtures of electrolytes inside nanopores. *J. Chem. Phys.* **2008,** *128*, 044705.

(39) Yang, C.; Hu, K.; Wang, D.; Zubi, Y.; Lee, S. T.; Puthongkham, P.; Mirkin, M. V.; Venton, B. J. Cavity Carbon Nanopipette Electrodes for Dopamine Detection. *Anal. Chem.,* DOI: *10.1021/acs.analchem.8b05885.*

For TOC only

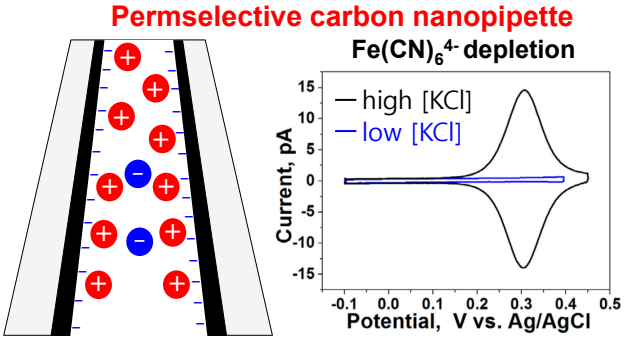
Permselective carbon nanopipette
Fe(CN)6 4- depletion
high [KCl]
low [KCl]
Current, pA
15
10
5
0
-5
-10
-15
-0.1
0.0
0.1
0.2
0.3
0.4
0.5
Potential, V vs. Ag/AgCl